# Movement-surface interactions of flying insects in three-dimensional space

Danish A. Ahmed[a, *], Ross N. Cuthbert[b], Isadora E. Fluck[c], Frances M. Hawkes[d], Gala Garrod[b]

[a] Department of Mathematics and Natural Sciences, Gulf University for Science and Technology, P.O. Box 7207, Hawally 32093, Kuwait.
[b] Institute for Global Food Security, School of Biological Sciences, Queen's University Belfast, 19 Chlorine Gardens, Belfast BT9 5DL, United Kingdom.
[c] School of Natural Resources and Environment, Department of Wildlife Ecology and Conservation, University of Florida, Gainesville, FL 32611, United States.
[d] Natural Resources Institute, University of Greenwich, London and South East University Group, Medway Campus, Central Avenue, Chatham Maritime, Kent ME4 4TB, United Kingdom.

*Corresponding author (Ahmed.D@gust.edu.kw)

**Abstract**

Three-dimensional movement is increasingly measurable for flying insects. However, modelling approaches have lagged behind, limiting mechanistic understanding of how flight behaviour influences interception by planar trapping surfaces. We simulate insect movement in three-dimensional space using biased and correlated random walks, distinguishing panel contact from edge leakage and accounting for repeated encounters and probabilistic retention upon contact. Using biologically plausible parameters for short-range flight by insects (such as whiteflies, thrips and mosquitoes), we examined how movement behaviour, panel size and retention jointly influence trapping outcomes. Encounter and capture probabilities increased with panel size relative to movement persistence length (the characteristic distance over which successive flight directions remain correlated), but remained low without directional bias, showing that larger panels cannot compensate for weak attraction. Stronger directional bias towards the panel increased encounters, repeated contacts and capture, whereas greater persistence generally reduced capture by producing straighter trajectories less readily redirected towards the panel, despite shortening time to first encounter among successful trajectories. Increasing retention enhanced capture but could not compensate for low encounter rates, while also truncating repeated-contact sequences. Interception failure due to edge leakage peaked at intermediate directional bias and greater persistence, and declined with stronger bias or larger panels. These results show that planar trap performance in flying insects depends jointly on movement behaviour, finite trap geometry and retention. The framework provides a mechanistic basis for interpreting trap catches, generating experimentally testable predictions, and exploring how context-specific differences in movement behaviour may influence planar trap performance across monitoring and control initiatives.

**Keywords** Three-dimensional movement, insect trapping, biased correlated random walk, directional persistence, directional bias, edge leakage, planar traps

## 1. Introduction

Growing interest has emerged in analysing flying insect movement in three-dimensional space (Zuo et al., 2026), facilitated by technological advances that are transforming insect ecology and monitoring (Van Klink et al., 2022). These include advances in high-resolution imaging (Dedic et al., 2024), multi-camera tracking systems (Batista et al., 2019; Bredt et al., 2025), lidar-based tracking (Kirkeby et al., 2016), and harmonic radar tags (Hurst et al., 2024), which increasingly allow behavioural and spatial patterns to be resolved that are difficult or impossible to capture from two-dimensional observations alone (Chen et al., 2024). Such approaches have been applied across a range of taxa, including vector mosquitoes (e.g. *Aedes aegypti*; Jimenez-Vallejo et al., 2026; *Anopheles gambiae*; Spitzen et al., 2013), fruit flies (e.g. *Drosophila melanogaster*; Vaxenburg et al., 2025), and bees (e.g. *Apis mellifera*; Sun and Gaydecki, 2021; *Bombus terrestris*; Stiemer et al., 2023), enabling detailed reconstruction of three-dimensional flight trajectories (Butail et al., 2012). Together, these advances provide a strong empirical foundation for three-dimensional insect movement, informing both ecological understanding and management, while motivating the development of theoretical movement models that link observed flight behaviour to ecological processes and outcomes (Ahmed et al., 2021; Lennox et al., 2025).

Despite recent advances in three-dimensional imagery approaches, modelling tools to analyse these data have not kept pace. While two-dimensional movement models have provided considerable insight for terrestrial insects (Petrovskii et al., 2014; Van Klinken et al., 2023; Ahmed et al., 2023b), with some applications to flying insects (Reynolds and Frye, 2007; Byers, 2012), their two-dimensional representation of movement is increasingly recognised as an oversimplification of airborne behaviours (Chen et al., 2021; Ahmed et al., 2023a). The vertical dimension influences flight behaviour, including differences between ascending and descending flight arising from gravitational and aerodynamic constraints (Shen et al., 2018; Walker and Taylor, 2021), as well as environmental exposure and encounters with ecological targets such as resources, conspecifics, and trapping surfaces (Wainwright et al., 2017; Jimenez-Vallejo et al., 2026). Accordingly, recent theoretical developments have extended movement models into three dimensions, particularly stochastic trajectory-based approaches such as biased and correlated random walks, enabling a more realistic representation of directional persistence, bias, and spatial exploration (Benhamou, 2018; Ahmed et al., 2021; Klappstein et al., 2026). Although knowledge gaps remain in the practical integration of random walk frameworks in three-dimensional contexts, these developments provide a theoretical basis for linking individual-level movement processes to emergent ecological processes in vertically structured environments.

One important practical application of three-dimensional movement modelling is insect trapping. Traps are widely used in ecological monitoring and pest management to assess population abundance, detect invasive species, and inform control strategies (Southwood, 1978; El-Sayed et al., 2006; Radcliffe et al., 2008). For flying insects, traps are typically elevated and often consist of finite planar surfaces, such as sticky panels or coloured cards. These planar surfaces attract individuals, induce a landing response or intercept individuals mid-flight (Epsky et al., 2008). Planar surfaces are also increasingly used *within* larger traps with more complex three-dimensional structures to monitor for pathogens, particularly in vector mosquitoes via baited FTA cards that enable surveillance from pooled

samples based on expectorated saliva (Manzi et al., 2023). Moreover, their practical application can be of significant public health importance. For instance, highly successful control campaigns against human African trypanosomiasis ('sleeping sickness') use insecticide-impregnated planar surfaces to attract and kill the tsetse fly vectors of *Trypanosoma* parasites (Esterhuizen et al., 2011; Bessell et al., 2021). These targets are carefully designed to incorporate the vector's known behavioural responses to specific visual features (Lindh et al., 2009) and have reduced disease incidence by up to 25% in some areas (Bessell et al., 2021). Although planar trap systems are widely used across taxa (e.g. aphids, whiteflies, thrips, and mosquitoes; Rehling et al., 2025; Roberts et al., 2025), the mechanistic relationship between trap catches and movement behaviour that generates encounters with trapping surfaces remains insufficiently characterised. In practice, trap counts are often interpreted as indices of abundance or activity, with limited consideration of the behavioural processes underlying encounter and capture, or the influence of trap placement and design. A stronger mechanistic understanding of how movement behaviour influences interception could improve interpretation of trap data and provide a basis for evaluating trap performance and improving their design (Ahmed et al., 2021).

From a theoretical perspective, trap encounter is a first-passage process in which a movement trajectory intersects a target region in space, while successful capture additionally depends on retention following contact. Consequently, trapping outcomes depend on the interaction between movement characteristics and trap geometry (Petrovskii et al., 2012; Ahmed and Petrovskii, 2019), and in broader monitoring contexts, the spatial configuration of traps (Hohbein and Conway, 2018; Ahmed et al., 2023b). Previous modelling studies have largely focused on two-dimensional systems, particularly pitfall traps for ground-dwelling insects, where links between movement processes and trap counts have been extensively explored (Petrovskii et al., 2014; Miller et al., 2015). Although three-dimensional approaches have been developed for specific trapping and encounter contexts (Byers, 2009; Cribellier et al., 2018), comparatively little attention has been given to general movement-based frameworks for planar interception by traps in three-dimensional space. Existing work has demonstrated that trap counts for three-dimensional volumetric traps depend nonlinearly on trap size and movement properties (Ahmed et al., 2021), but a mechanistic framework for planar interception remains lacking, despite the widespread use of panel traps in practice. Empirical studies further indicate that flying insect movement is structured and influenced by multiple interacting drivers, including environmental conditions, visual and olfactory cues, and physiological state (Wainwright et al., 2017). For example, mosquito flight behaviour exhibits strong responses to microclimatic gradients and visual, thermal or olfactory stimuli, leading to non-uniform space use, sensory synergisms and directional bias (Carnaghi et al., 2021; Jimenez-Vallejo et al., 2026). Infection or reproductive status of vectors has also been shown to alter flight speed and distance along with general locomotor activity (Lima-Camara et al., 2011; Somerville et al., 2019; Tallon et al., 2020; Dong et al., 2025). Such inputs operate over different spatial scales and interact with each other in non-linear ways, and the emergent behaviours can directly influence the probability of encountering and interacting with a trap surface (Spitzen et al., 2013; van Breugel et al., 2015; Carnaghi et al., 2024). Therefore, a mechanistic understanding of trapping requires integrating context-dependent movement dynamics with the finite geometry and potential attractant properties of trapping

surfaces.

We develop a three-dimensional modelling framework for insect trapping by planar surfaces based on correlated and biased correlated random walks. Movement is represented as a stochastic process with directional persistence and directional bias towards a target, while trapping is formulated geometrically as the intersection between trajectories and a finite panel. Within this framework, we examine how panel size, directional persistence, bias and retention influence panel encounters, repeated contact, capture probability and time to first encounter, together with edge leakage, defined as crossing the panel plane outside the finite panel boundaries. We further examine panel size relative to the persistence length of movement to characterise how movement scale and trap geometry jointly influence interception. This work provides a mechanistic link between three-dimensional movement processes and trapping outcomes, offering a basis for interpreting trap catches and exploring how movement behaviour, trap geometry and retention jointly influence the performance of planar trapping surfaces. More broadly, it contributes to the development of three-dimensional movement ecology by showing how movement behaviour, finite panel geometry and post-contact retention interact to determine trapping outcomes.

## 2. Methods

The modelling framework simulates insect movement in three-dimensional space using biased and correlated random walks, incorporating directional persistence and attraction towards a finite planar trapping surface, representing responses to trap-associated environmental cues. The model accounts for panel encounters, repeated contacts, probabilistic retention upon contact, and edge leakage when flight paths cross the panel plane but miss the trapping surface.

### 2.1 *Three-dimensional random walk movement model*

We model individual insect movement as a discrete-time stochastic process in three-dimensional Cartesian space. The position of an individual after movement step $i$ is denoted by $\mathbf{x}_i = (x_i, y_i, z_i)$, and successive locations are connected by the displacement vector $\Delta\mathbf{x}_i = \mathbf{x}_i - \mathbf{x}_{i-1}$. The corresponding step length is $l_i = \|\Delta\mathbf{x}_i\|$, while the direction of movement is represented by the unit heading vector $\mathbf{u}_i = \Delta\mathbf{x}_i / l_i$. Positions are updated at fixed time intervals $\Delta t$ according to

$$\mathbf{x}_i = \mathbf{x}_{i-1} + l_i\mathbf{u}_i. \quad (1)$$

The resulting trajectory is therefore represented as a sequence of straight-line displacements over fixed movement intervals $\Delta t$, with the step length and heading specified probabilistically at each movement update. The corresponding velocity vector is given by $\mathbf{v}_i = l_i\mathbf{u}_i/\Delta t$, which accounts for both flight speed and direction.

For the baseline isotropic movement process, the Cartesian components of each displacement are assumed to be mutually independent Gaussian random variables with zero mean and the same standard deviation $\sigma$, such that $\Delta x_i, \Delta y_i, \Delta z_i \overset{\text{iid}}{\sim} \mathcal{N}(0, \sigma^2)$. The parameter $\sigma$ therefore controls the characteristic spatial scale of movement during one time interval $\Delta t$. Under these assumptions, the displacement vector is isotropically distributed, and the step length follows a Maxwell distribution,

$$\lambda(l) = \frac{2l^2}{\sigma^3\sqrt{2\pi}} \exp\left(-\frac{l^2}{2\sigma^2}\right), \quad l > 0 \tag{2}$$

which is equivalent to the variable $l/\sigma$ following a chi distribution with three degrees of freedom. The mean and mean-squared step lengths are

$$\mathbb{E}(l) = \frac{4\sigma}{\sqrt{2\pi}}, \ \mathbb{E}(l^2) = 3\sigma^2, \tag{3}$$

respectively. The corresponding variance is $\mathrm{var}(l) = \left(3 - \frac{8}{\pi}\right)\sigma^2$, and the coefficient of variation is $\sqrt{\frac{3\pi}{8} - 1}$.

Because the three Cartesian increments are independent and identically distributed, the isotropic process has no preferred direction. The heading vector is therefore uniformly distributed over the surface of the unit sphere. In spherical coordinates, the azimuthal angle $\theta_i \in (-\pi, \pi]$ is uniformly distributed, while the polar angle $\phi_i \in [0, \pi]$ has probability density $\frac{1}{2}\sin(\phi_i)$. The displacement components may then be written as

$$\Delta x_i = l_i \cos(\theta_i)\sin(\phi_i), \Delta y_i = l_i \sin(\theta_i)\sin(\phi_i), \text{ and } \Delta z_i = l_i \cos(\phi_i). \tag{4}$$

For an unbiased and uncorrelated walk, the mean-squared displacement (MSD) after $n$ steps is

$$\mathrm{MSD} = \mathbb{E}[\|\mathbf{x}_n - \mathbf{x}_0\|^2] = n\mathbb{E}(l^2) = 3n\sigma^2. \tag{5}$$

Since the elapsed time is $t = n\Delta t$, comparison with the three-dimensional diffusion relation $\mathrm{MSD} = 6Dt$ gives the effective diffusion coefficient $D = \frac{\sigma^2}{2\Delta t}$. Hence, $\sigma$ determines both the typical displacement per movement update and the long-term rate of spatial spread. This formulation follows the three-dimensional random walk framework used for animal movement and encounter processes (Ahmed et al., 2021).

### 2.2 *Directional updating through persistence and panel-oriented bias*

Let $\mathbf{u}_{i-1}$ denote the unit heading vector of the previous step. The direction of step $i$ was determined by combining persistence in the previous direction with attraction towards the panel. The resulting directional vector was defined as

$$\mathbf{m}_i = \kappa_p \mathbf{u}_{i-1} + \kappa_b \mathbf{g}_i, \tag{6}$$

where $\kappa_p \geq 0$ controls directional persistence, $\kappa_b \geq 0$ controls the strength of attraction towards the panel, and $\mathbf{g}_i$ is the unit vector pointing from the individual's current position towards its assigned target on the panel. In the biased movement model, each trajectory is assigned a fixed target point, while $\mathbf{g}_i$ is recalculated at every step as the individual moves. The attraction parameter $\kappa_b$ represents the net directional response to trap-associated environmental cues, without distinguishing between individual sensory mechanisms.

The resultant vector $\mathbf{m}_i$ determines both the mean direction and concentration of the vMF distribution. Provided that $\|\mathbf{m}_i\| > 0$, these are given by

$$\boldsymbol{\mu}_i = \frac{\mathbf{m}_i}{\|\mathbf{m}_i\|}, \qquad \kappa_i = \|\mathbf{m}_i\|. \tag{7}$$

The new heading is then sampled according to

$$\mathbf{u}_i \sim \mathrm{vMF}(\boldsymbol{\mu}_i, \kappa_i), \tag{8}$$

with density

$$f(\mathbf{u}_i|\boldsymbol{\mu}_i, \kappa_i) = \frac{\kappa_i}{4\pi \sinh(\kappa_i)} \exp\left(\kappa_i \boldsymbol{\mu}_i^{\mathrm{T}} \mathbf{u}_i\right). \tag{9}$$

The parameter $\kappa_i$ controls angular concentration around $\boldsymbol{\mu}_i$. Small values produce widely dispersed headings, whereas larger values produce headings more closely aligned with the resultant direction. Because $\kappa_i = \|\mathbf{m}_i\|$, the concentration is not necessarily constant: it increases when persistence and attraction act in similar directions and decreases when they oppose one another.

When $\kappa_b = 0$, Eq. (6) reduces to $\mathbf{m}_i = \kappa_p \mathbf{u}_{i-1}$, so that movement is governed solely by short-term directional persistence and the process is a three-dimensional correlated random walk (CRW). When $\kappa_b > 0$, the new heading reflects a compromise between persistence and attraction towards the panel, producing a biased correlated random walk (BCRW). In the absence of both components, $\kappa_p = \kappa_b = 0$ and hence $\|\mathbf{m}_i\| = 0$; the heading is then sampled uniformly over the unit sphere, corresponding to an unbiased simple random walk (Ahmed et al., 2021; Klappstein et al., 2026).

### 2.3 *Persistence length*

For the CRW, directional persistence is quantified using the mean cosine of the angle between successive headings in the absence of directional bias. When the new heading is sampled from a three-dimensional von Mises–Fisher (vMF) distribution centred on the previous heading with concentration parameter $\kappa_p$, the directional correlation is

$$\rho = \coth(\kappa_p) - \frac{1}{\kappa_p}. \tag{10}$$

Here, $\rho$ measures the expected alignment between successive headings: $\rho = 0$ corresponds to no directional persistence, whereas values approaching 1 indicate increasingly straight movement. This relationship follows directly from the mean resultant length of the three-dimensional vMF distribution (Mardia and Jupp, 2000).

For a CRW with constant directional correlation, the expected correlation between headings separated by $k$ steps decays geometrically as $\rho^k$. The corresponding characteristic persistence time, measured in numbers of steps, is therefore $n_p = -\frac{1}{\log(\rho)}$. Multiplying this by the mean step length gives the persistence length,

$$l_p = -\frac{\mathbb{E}(l)}{\log(\rho)}. \tag{11}$$

Using the step-length distribution given in equation (3), the persistence length becomes

$$l_p = -\frac{4\sigma}{\sqrt{2\pi}\log(\rho)}. \tag{12}$$

The persistence length therefore represents the characteristic distance over which the effect of the previous heading is retained. Larger values of $\kappa_p$ produce larger values of $\rho$ and hence longer persistence lengths, whereas $\kappa_p \to 0$ gives $\rho \to 0$, corresponding to an uncorrelated random walk. In the BCRW, the realised direction depends on both the previous heading and attraction towards the panel. Consequently, the correlation between successive headings is no longer determined by $\kappa_p$ alone. For consistency, we therefore define $l_p$ using the corresponding baseline correlated random walk with $\kappa_b = 0$. This isolates the intrinsic persistence of the movement process from the additional effect of directional attraction.

### 2.4 *Panel-target specification*

For biased movement, each individual was assigned a fixed target point selected uniformly at random over the panel surface, allowing for variation in where insects orient towards the panel, while assuming no spatial differences in attractiveness across its surface. For a rectangular panel of width $W$ and height $H$, centred at the origin in the plane $x = 0$, the target was defined by

$$y_{\text{tar}} \sim \text{Unif}\left(-\frac{W}{2}, \frac{W}{2}\right),\ z_{\text{tar}} \sim \text{Unif}\left(-\frac{H}{2}, \frac{H}{2}\right),\ \text{with } \mathbf{q} = (0, y_{\text{tar}}, z_{\text{tar}}). \quad (13)$$

The target remained fixed during the individual's approach to the panel. At step $i$, the direction of attraction was the unit vector pointing from the current position $\mathbf{x}_{i-1}$ towards $\mathbf{q}$:

$$\mathbf{g}_i = \frac{\mathbf{q}-\mathbf{x}_{i-1}}{\|\mathbf{q}-\mathbf{x}_{i-1}\|}. \quad (14)$$

Assigning targets across the panel surface represents attraction towards the panel as an extended object, rather than concentrating all trajectories towards its centre. Directional attraction was removed after the trajectory first interacted with, or passed through, the panel plane, representing the loss of attraction following an initial approach event, after which movement continued as a CRW. In the numerically degenerate case where $\|\mathbf{q} - \mathbf{x}_{i-1}\|$ was effectively zero, $\mathbf{g}_i$ was replaced by the panel-normal unit vector $(1, 0, 0)$.

### 2.5 *Initial conditions and trajectory termination*

Individuals were released uniformly within a circular region of radius $R$ in the plane $x = -d$. Uniform sampling over the release disc was achieved by drawing

$$r = R\sqrt{U},\ U \sim \text{Unif}(0, 1),\ \text{together with } \psi \sim \text{Unif}(0, 2\pi). \quad (15)$$

The initial position is then

$$\mathbf{x}_0 = (-d, r\cos\psi, r\sin\psi). \quad (16)$$

Initial headings were sampled uniformly over the unit sphere. Thereafter, positions were updated according to Eq. (1). Each trajectory was simulated for a maximum of $n_{\max}$ movement steps and was terminated earlier if the individual left the computational domain, defined by

$$x_i > x_{\max},\ x_i < x_{\min},\ \text{or}\ \|\mathbf{x}_i\| > R_{\text{escape}}. \tag{17}$$

Thus, a trajectory ended upon capture, escape from the computational domain, or completion of the maximum number of movement steps.

### 2.6 *Panel interception, capture, and post-contact movement*

The trap was represented as a finite rectangular panel centred at the origin in the plane $x = 0$, with width $W$ in the $y$-direction and height $H$ in the $z$-direction. The panel therefore occupied the region

$$|y| \le \frac{W}{2},\ |z| \le \frac{H}{2}. \tag{18}$$

At each movement step, the line segment joining the successive positions $\mathbf{x}_i$ and $\mathbf{x}_{i+1}$ was tested for intersection with the plane $x = 0$. If the segment crossed this plane, the intersection parameter was calculated as

$$\tau = -\frac{x_i}{x_{i+1} - x_i}, \tag{19}$$

where $x_i$ and $x_{i+1}$ denote the $x$-coordinates of the two positions, and $0 \le \tau \le 1$ specifies the location of the intersection along the movement segment. The corresponding intersection point was

$$\mathbf{x}_{\text{int}} = \mathbf{x}_i + \tau(\mathbf{x}_{i+1} - \mathbf{x}_i). \tag{20}$$

An intersection was classified as contact with the panel when

$$|y_{\text{int}}| \le \frac{W}{2},\ |z_{\text{int}}| \le \frac{H}{2}. \tag{21}$$

If the segment crossed the plane outside these bounds, the event was classified as edge leakage. In this case, no contact occurred, attraction towards the panel was removed, and the trajectory continued as a CRW. When contact occurred, the attempted movement step was truncated at $\mathbf{x}_{\text{int}}$. The individual was then captured with probability $p_{\text{stick}}$, in which case the trajectory terminated at the contact point. Otherwise, a post-contact heading $\mathbf{u}_{\text{post}}$ was sampled from a vMF distribution centred on the outward panel normal, $\boldsymbol{\mu}_{\text{post}} = (-1, 0, 0)$, with concentration parameter $\kappa_{\text{post}}$. Sampling was restricted to headings satisfying $u_{\text{post},x} < 0$, so that the individual moved away from the panel after failed capture.

To prevent immediate numerical re-contact, the position was displaced slightly from the panel according to

$$\mathbf{x} = \mathbf{x}_{\text{int}} + \varepsilon \mathbf{u}_{\text{post}}, \tag{22}$$

where $\varepsilon > 0$ is a small displacement constant. A new step length was then sampled, and movement continued using $\mathbf{u}_{\text{post}}$ as the reference heading. Panel-oriented attraction was removed after the first interaction with the panel plane, but subsequent intersections with the

finite panel could still occur through the correlated movement process. Thus, failed capture could generate repeated contact opportunities, whereas edge leakage represented crossing the panel plane outside the finite trapping surface without interception. All simulations were implemented in MATLAB R2016a.

### 2.7 *Simulation design and ecological parametrisation*

While flight behaviours vary among species and individuals and are highly context-dependent (Martínez-Pérez et al., 2022; Oram and Card, 2022; Polidori et al., 2022; MacLeod and Luong, 2024), the relative conservation of wingbeat kinematics across dipteran taxa, despite substantial variation in wing and body morphology, suggests that similar aerodynamic principles may govern aspects of dipteran flight (Le Roy et al., 2026). We therefore selected parameters to represent short-range flight by relatively small insects interacting with a finite panel-type trap, rather than to reproduce the behaviour of a specific species.

Spatial quantities were expressed in centimetres and time in seconds. The baseline movement interval was $\Delta t = 0.02$ s, providing fine temporal resolution for changes in flight direction near the panel (Ings and Chittka, 2008). A nominal mean flight speed of $v = 25$ cm $s^{-1}$ was used, consistent with the order of magnitude reported for short-range flight in small insects. For example, mean horizontal forward speeds of approximately 24 cm $s^{-1}$ have been reported for *Bemisia tabaci*, while *Anopheles gambiae* reached a mean ground speed of 27 cm $s^{-1}$ under combined odour and heat cues (Isaacs et al., 1999; Spitzen et al., 2013). This corresponds to a mean step length of $\mathbb{E}(l) = v\Delta t = 0.5$ cm. The selected speed was intended as a phenomenological baseline rather than a species-specific calibration, allowing the effects of panel size, directional persistence and movement bias to be examined independently. Although absolute spatial and temporal scales would vary with flight speed, the qualitative relationships among these movement and trapping parameters are expected to be broadly retained. Using the mean step length given in Eq. (3), the corresponding scale parameter was $\sigma \approx 0.313$ cm. These values therefore define the baseline spatial and temporal scale of the simulations rather than an exact representation of flight behaviour for any particular species.

Directional persistence and bias were varied over ranges intended to represent contrasting short-range flight behaviours rather than species-specific fitted estimates. Directional persistence was explored from $\kappa_p = 0$, corresponding to no directional persistence, to $\kappa_p = 5$, producing strongly persistent and relatively straight movement. Such variation allows the model to represent contrasting degrees of directional continuity and is consistent with observed insect search behaviour. For example, starved fruit flies (*Drosophila melanogaster*) explore their surroundings for resources through a series of relatively straight flight segments separated by rapid turns, with the resulting movement pattern consistent with a Lévy-like search strategy (Reynolds and Frye, 2007). The encounter with a cue can then modify this exploratory behaviour, introducing directional bias into the insect's movement and guiding it toward a resource or other biologically relevant target (Reynolds and Frye, 2007; Reynolds and Rhodes, 2009). In our model, directional bias was varied from $\kappa_b = 0$, representing no attraction towards the panel, to $\kappa_b = 1$, representing strong orientation towards the target. This parameter represents the overall tendency to orient towards the panel in response to environmental cues, rather than explicitly modelling specific flight behaviours

such as upwind orientation, casting or visually guided turns. Olfactory cues from floral resources, for example, were observed to provide directional information during bumblebee (*Bombus terrestris*) foraging, with more experienced individuals showing a tendency to fly upwind toward specific floral resources (Osborne et al., 2013). Therefore, the ranges of both $\kappa_p$ and $\kappa_b$ parameters were chosen to span contrasting movement behaviours (i.e., weakly structured, persistent and strongly biased) while retaining stochastic variation in heading, thereby capturing key features of the variation in flight patterns and directional responses observed across insects in different ecological contexts.

The trapping surface was represented by a finite square panel, with $L = 10$ cm used as a representative panel size and $L$ varied in some analyses to examine the effect of panel size. Practical sticky cards are often rectangular and measure approximately $10 \times 20$ or $10 \times 25$ cm, with larger formats also available (Pobozniak et al., 2020). Square geometry was adopted to simplify the model and facilitate scaling of panel size relative to movement persistence.

The simulations were designed to represent short-term, short-range flight during local approach to a planar trapping surface rather than long-range dispersal. Individuals were released at distances on the order of tens of centimetres from the panel, with distances up to 1 m considered when examining the effect of approach distance. These distances represent the local spatial scale over which insects may detect, orient towards, or otherwise respond to the surface. Individuals were released uniformly across a finite circular release region of radius $R$ in the plane $x = -d$, rather than from a single point, thereby incorporating spatial variation in the location and angle of approach. In the primary simulations, the release region had radius $R = 20$ cm, giving a diameter four times the baseline panel width ($L = 10$ cm). This provided a spatially dispersed source of insects while retaining a local scale relevant to short-range panel approach. This design reduced dependence on a highly constrained initial configuration and allowed interception outcomes to arise from the interaction between movement behaviour and finite panel geometry.

The framework has broad ecological and agricultural relevance, since planar trapping surfaces are widely used to estimate insect abundance or activity and to inform population monitoring, pest management and vector surveillance (Heinz et al., 1992; Roberts et al., 2025). For example, continuous monitoring of *Aedes aegypti* using sticky traps provides abundance indices capable of tracking seasonal population dynamics and predicting dengue disease occurrence (Da Cruz Ferreira et al., 2017). However, contact with a sticky trap does not necessarily result in retention. When testing the efficiency of yellow sticky traps, agricultural pests such as western flower thrips (*Frankliniella occidentalis*) can escape after initial contact, with escape depending on adhesive properties (Rehling et al., 2025). This highlights the need to account for imperfect retention when designing insect monitoring and abundance estimation strategies using planar traps, a broadly applicable methodology for a wide range of insects of agricultural importance (Benthall et al., 2022). To account for variation in capture following contact across sticky and other panel-like trapping methodologies, the model includes a conditional probability of retention following contact, $p_{\mathrm{stick}}$, which can represent incomplete adhesion, escape after impact, surface deterioration or other trap-specific factors affecting retention. Similar distinctions between attraction and

successful capture have been demonstrated for mosquito suction traps (Cribellier et al., 2018, 2020). In our simulations, an intermediate value of $p_{\mathrm{stick}} = 0.5$ was used as a representative retention probability, while values from 0 to 1 were explored to span the full range from complete capture failure to certain retention after contact.

### 2.8 *Characteristic movement scale relative to panel distance*

For independent step lengths and directional correlation $\rho$, the large-$n$ mean squared displacement of the baseline CRW is

$$\mathrm{MSD} \approx n\left[\mathbb{E}(l^2) + 2\mathbb{E}(l)^2 \cdot \frac{\rho}{1-\rho}\right]. \tag{23}$$

Because the baseline CRW is isotropic, one third of this displacement is associated with the panel-normal direction. Thus, $\mathrm{MSD}_x = \frac{1}{3}\mathrm{MSD}$ and the corresponding characteristic displacement along the $x$-axis is $\sqrt{\mathrm{MSD}_x}$. For $\sigma = 0.313$ cm and $\kappa_p = 3$, this gives characteristic panel-normal displacements of approximately 11.5 cm after 300 steps and 14.8 cm after 500 steps.

A baseline reachability scale can then be obtained by setting the characteristic panel-normal displacement equal to the initial panel offset, $\sqrt{\mathrm{MSD}_x} \approx d$. This gives

$$n_{\mathrm{reach}} \approx 3d^2\left[\mathbb{E}(l^2) + 2\mathbb{E}(l)^2 \cdot \frac{\rho}{1-\rho}\right]^{-1}. \tag{24}$$

with the corresponding characteristic time given by $t_{\mathrm{reach}} = n_{\mathrm{reach}}\Delta t$. This provides a baseline of a characteristic number of steps, or elapsed time, required for the typical displacement of an unbiased CRW to become comparable to the distance from the panel. It is not a first-passage time or a guarantee of contact, since individual trajectories may reach the panel earlier, later or not at all. This applies only to the baseline CRW, because directional bias introduces a systematic tendency towards the panel.

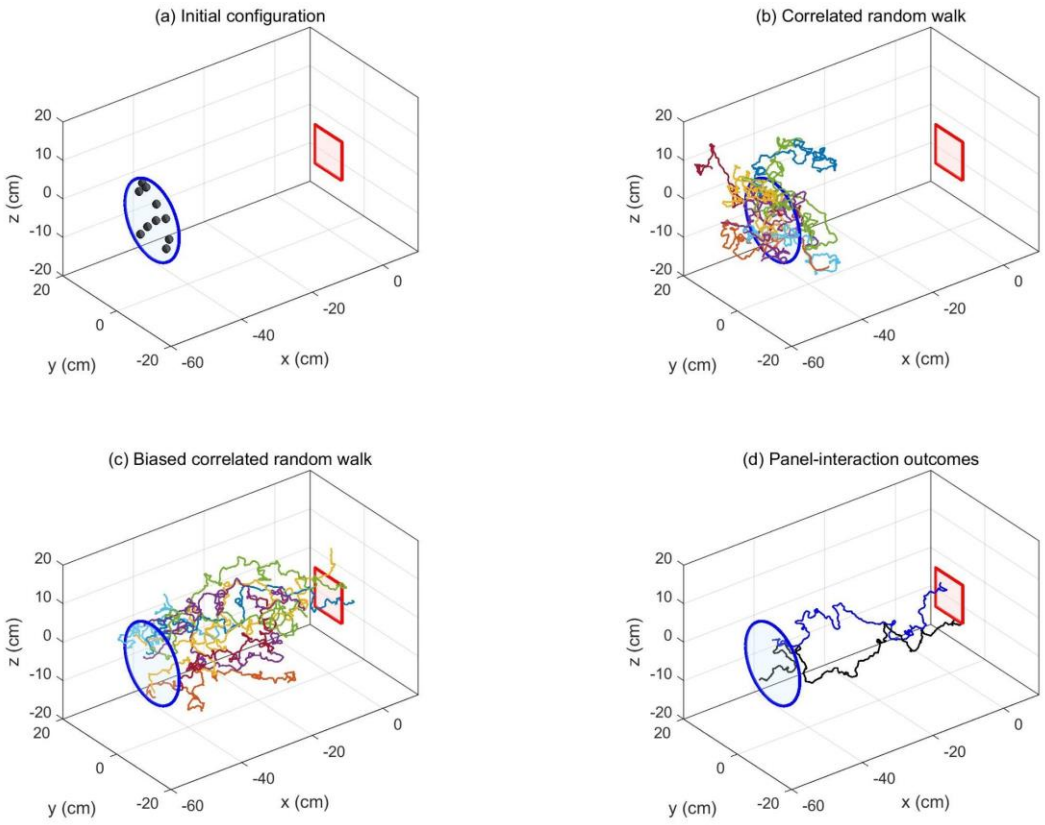



**Figure 1.** Three-dimensional illustration of the movement and panel-interaction framework. (a) Initial configuration, showing 10 positions sampled uniformly within a circular release region of radius $R = 10$ cm in the plane $x = -d = -50$ cm. The square panel is centred at the origin in the plane $x = 0$, with $W = H = 10$ cm. (b) Example trajectories generated by a correlated random walk with directional persistence $\kappa_p = 3$ and no panel-oriented bias ($\kappa_b = 0$). (c) Example trajectories generated by a biased correlated random walk with $\kappa_p = 3$ and bias strength $\kappa_b = 0.5$, where each trajectory is assigned a fixed target selected uniformly over the panel surface. Directional bias is removed after the trajectory first intersects or crosses the panel plane. (d) Representative outcomes from the full panel-interaction model: capture following contact with the panel (blue) and edge leakage following passage through $x = 0$ outside the panel boundaries (black). Across all panels, the step-length scale was $\sigma = 0.313$ cm, the movement interval was $\Delta t = 0.02$ s, and trajectories were simulated for at most $n_{\max} = 300$ steps, corresponding to duration 6 s. For panel (d), the probability of capture following contact was $p_{\text{stick}} = 0.5$, the post-contact directional concentration was $\kappa_{\text{post}} = 5$, and the numerical displacement used to prevent immediate re-contact was $\varepsilon = 10^{-3}$ cm.

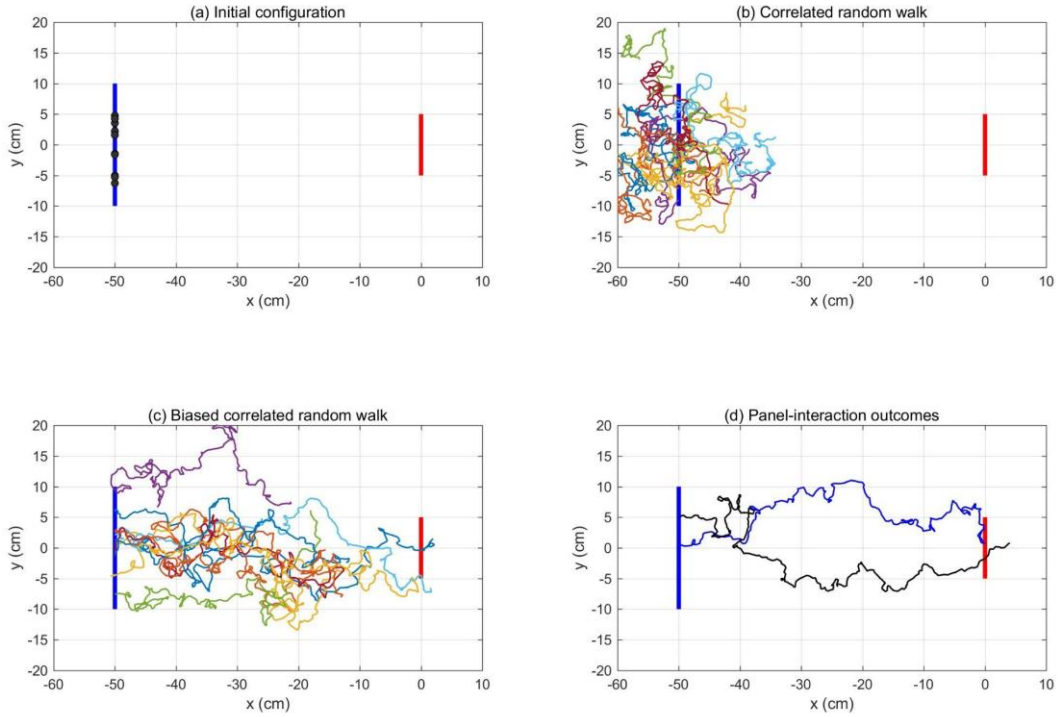



**Figure 2.** Two-dimensional projection of the movement and panel-interaction framework onto the $x, y$ plane. Panels (a–d) show the same trajectory realisations and parameter values as Figure 1. The projection shows movement towards the panel along the $x$-axis and lateral displacement along the $y$-axis, with variation in the $z$-direction omitted. In panel (d), the blue trajectory represents capture following panel contact, whereas the black trajectory represents edge leakage through the plane $x = 0$ outside the panel boundaries.

## 3. Results

### 3.1 *Encounter probability and panel size–persistence scaling*

Both encounter probability (Figure 3a) and capture probability (Figure 3b) increased with panel size relative to the persistence length of movement. Here, encounter probability is the probability that a trajectory intersects the finite panel, whereas capture probability is the probability of eventual retention following panel contact. Encounter probability increased nonlinearly with the panel size–persistence ratio $\nu$, with the largest gains occurring at lower values of $\nu$ and progressively smaller gains at larger values. However, increasing panel size alone produced only limited interception in the absence of directional bias $\kappa_b = 0$, with encounter probabilities remaining low across the full range of $\nu$. In contrast, increasing $\kappa_b$ substantially elevated encounter probability at all panel sizes, with stronger bias producing consistently higher probabilities across the entire range. Thus, the effect of panel size depended strongly on movement behaviour rather than on geometry alone.

Capture probability showed the same overall dependence on $\nu$ and $\kappa_b$, but remained lower than encounter probability under intermediate retention $p_{\text{stick}} = 0.5$. For each value of $\kappa_b$, the capture curve closely followed the corresponding encounter curve. Thus, imperfect retention reduced the magnitude of trapping success, while the overall dependence of capture on panel size and directional bias largely reflected the underlying encounter process.

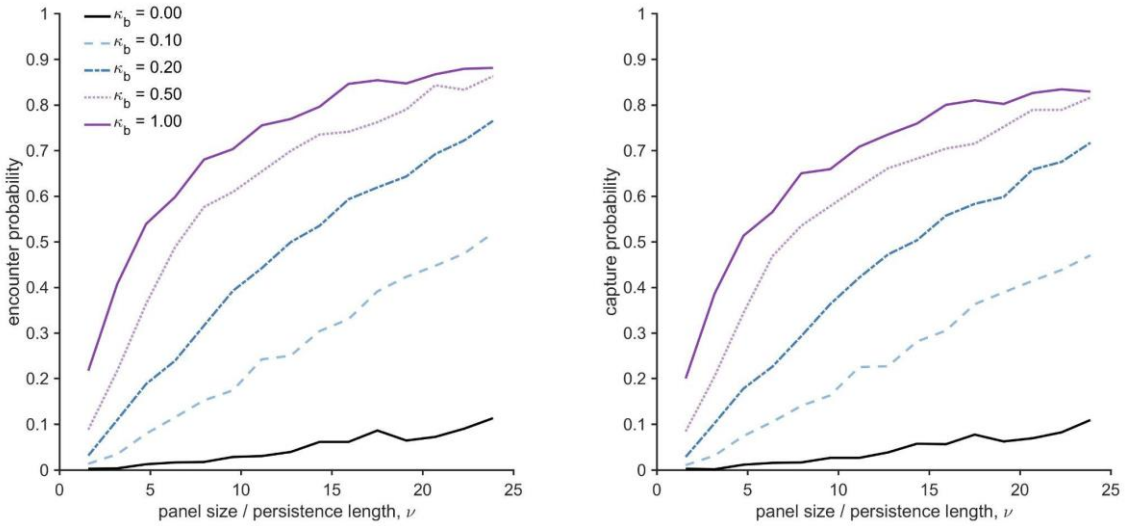



**Figure 3.** (a) Encounter probability and (b) capture probability as functions of the panel size–persistence ratio $\nu = L/l_p$, where $L$ is the side length of the square panel and $l_p$ is the persistence length of the baseline correlated random walk (equation 12). An encounter occurs when a trajectory intersects the finite panel, whereas capture denotes retention following panel contact; crossings of the panel plane outside the panel boundaries are classified as edge leakage. Panel side length was varied from $L = 2$ to 30 cm in 2 cm increments. Directional persistence was fixed at $\kappa_p = 3$, while directional bias was varied across $\kappa_b = 0, 0.1, 0.2, 0.5$ and 1. Movement used a time step $\Delta t = 0.02$ s and mean step length $\mathbb{E}(l) = 0.5$ cm, corresponding to a step-length scale parameter $\sigma = 0.313$ cm. Individuals were released from a circular region of radius $R = 20$ cm at $d = 30$ cm. Capture following contact occurred with probability $p_{\text{stick}} = 0.5$, with failed contacts followed by post-contact movement with $\kappa_{\text{post}} = 5$ and $\varepsilon = 10^{-3}$ cm. Trajectories were simulated for a maximum of 2500 steps or until capture or escape, and probabilities were estimated from 1000 independent trajectories for each parameter combination.

### 3.2 *Contact frequency and repeated panel interactions*

Contact frequency varied with panel size, directional bias, and retention (Figure 4). In the absence of retention $p_{\text{stick}} = 0$, the mean number of contacts increased with panel side length $L$ across all values of $\kappa_b$, although the magnitude of this increase was strongly bias-dependent (Figure 4a). Contact frequencies remained low for $\kappa_b = 0$, even for large panels, whereas increasing directional bias produced progressively higher numbers of contacts. Under strong bias, repeated interactions became common, with mean contact numbers exceeding five for the largest panels. At larger $L$, the curves for $\kappa_b = 0.5$ and 1 converged, indicating diminishing increases in contact frequency at high bias. The contact-count distributions at $L = 10$ cm showed the same shift in interaction structure (Figure 4b): unbiased trajectories were dominated by zero-contact outcomes, whereas increasing $\kappa_b$ reduced the probability of no contact and increased the probability of one or more contacts, with higher bias producing broader distributions and more frequent repeated interactions.

When retention was introduced at $p_{\text{stick}} = 0.5$, mean contact frequency remained positively related to both $L$ and $\kappa_b$, but was substantially reduced relative to the non-retentive case (Figure 4c). This reduction reflects termination of trajectories following successful capture, thereby limiting subsequent contact opportunities. Under stronger bias, mean contact

numbers approached a plateau at larger panel sizes, with little additional increase beyond intermediate values of $L$. The corresponding contact-count distributions were compressed towards zero and one contact (Figure 4d), with multiple-contact events becoming markedly less frequent than under $p_{\text{stick}} = 0$. Retention therefore altered the structure of panel interaction by truncating trajectories that would otherwise have contributed to repeated contacts.

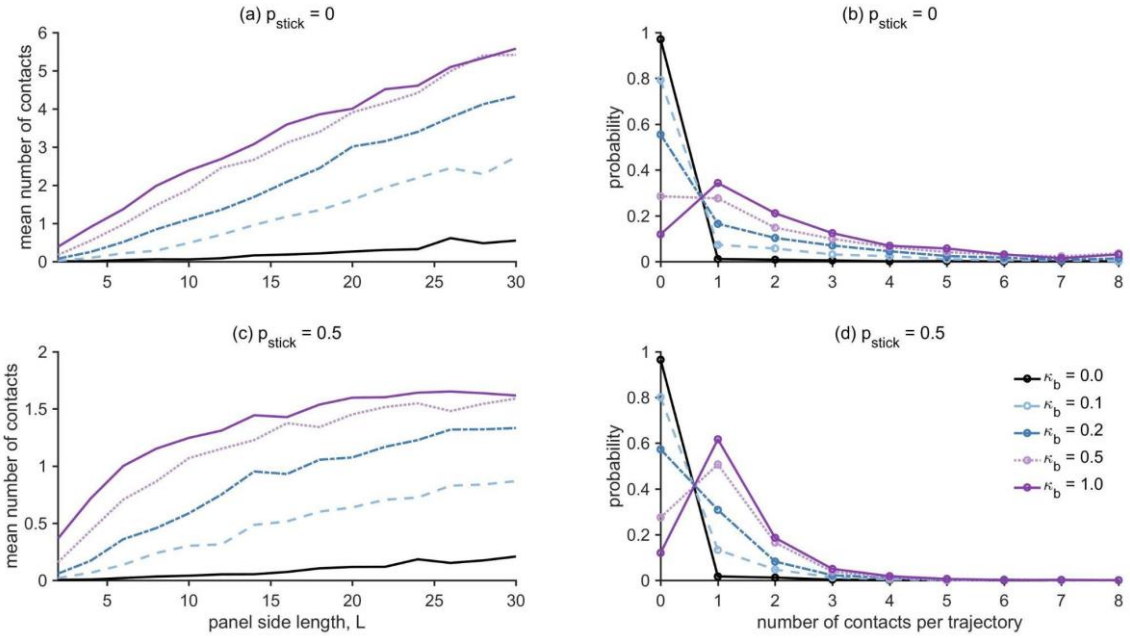



**Figure 4.** (a, c) Mean number of panel contacts per trajectory as a function of panel side length $L$, and (b, d) corresponding contact-count distributions for $L = 10$ cm. Directional bias was varied across $\kappa_b = 0, 0.1, 0.2, 0.5$ and 1. Panels (a, b) show no retention $p_{\text{stick}} = 0$, whereas panels (c, d) show intermediate retention $p_{\text{stick}} = 0.5$. Panel side length ranged from $L = 2$ to 30 cm in 2 cm increments in panels (a) and (c). Individuals were released from a circular region of radius $R = 20$ cm at $d = 30$ cm, and trajectories were simulated for a maximum of 2500 steps or until capture or escape. Each parameter combination was simulated using $N = 1000$ independent trajectories. All movement parameters were as in Figure 3.

### 3.3 *Bias–persistence trade-offs in capture probability*

Capture probability varied jointly with directional persistence $\kappa_p$, directional bias $\kappa_b$, and retention $p_{\text{stick}}$ (Figure 5). Across all retention levels, capture increased with $\kappa_b$ but generally declined with increasing $\kappa_p$. Consequently, high capture was concentrated at combinations of strong directional bias and low persistence, whereas weak bias and strong persistence produced consistently low capture. The contour structure reflected this interaction, with progressively greater $\kappa_b$ required to maintain a given capture probability as $\kappa_p$ increased. This pattern is consistent with stronger persistence producing straighter, more ballistic trajectories that are less readily redirected towards the finite panel, particularly when their initial directions are not aligned with the target, while directional bias counteracts this effect by maintaining attraction towards the target.

Increasing $p_{\text{stick}}$ expanded the region of parameter space associated with moderate and high capture. At $p_{\text{stick}} = 0.1$, capture remained low across most combinations of $\kappa_p$ and

$\kappa_b$, with the 25% contour largely restricted to strong bias and relatively low persistence (Figure 5a). At $p_{\text{stick}} = 0.5$ and 0.9, the 25%, 50%, and 75% contours extended progressively towards weaker bias and higher persistence (Figure 5b–c), indicating that improved retention reduced, but did not eliminate, the movement constraints on capture. Thus, retention increased overall capture while preserving a strong dependence on the balance between directional bias and persistence.

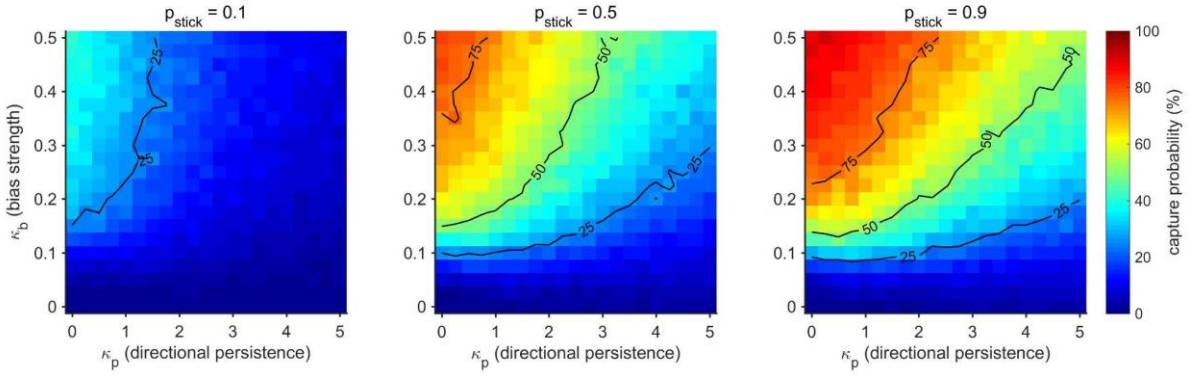



**Figure 5.** Heat maps showing capture probability as a function of directional persistence $\kappa_p$ and directional bias $\kappa_b$ for three values of the sticking probability: (a) $p_{\text{stick}} = 0.1$, (b) $p_{\text{stick}} = 0.5$ and (c) $p_{\text{stick}} = 0.9$. The panel was square with side length $L = 10$ cm, and capture probabilities were estimated from 1000 independent trajectories for each parameter combination. Contours indicate 25%, 50%, and 75% capture probability. Release conditions, trajectory duration, and all other movement and post-contact parameters were as in Figure 3.

### 3.4 *Retention-mediated capture dynamics*

Capture probability increased with $p_{\text{stick}}$ across all movement regimes, but the magnitude of this increase depended strongly on directional bias and persistence (Figure 6). At fixed $\kappa_p = 3$, increasing $\kappa_b$ produced a pronounced upward separation of the capture curves across the full range of $p_{\text{stick}}$ (Figure 6a). In the absence of bias, capture remained low even as $p_{\text{stick}}$ approached unity, whereas stronger bias substantially increased capture and produced diminishing gains at higher retention. Thus, increasing retention alone did not compensate for movement conditions that generated few panel encounters.

At fixed $\kappa_b = 0.2$, capture probability declined progressively with increasing directional persistence (Figure 6b). Low-persistence trajectories achieved the highest capture probabilities across most of the $p_{\text{stick}}$ range, whereas strong persistence substantially limited capture even under high retention, consistent with straighter, more ballistic trajectories reducing opportunities for panel interception and re-contact. The separation between persistence levels increased as $p_{\text{stick}}$ increased, indicating that the benefit of improved retention depended on the underlying probability of encountering the panel. Retention therefore amplified differences generated by movement behaviour rather than eliminating them, with directional bias promoting capture and strong persistence constraining the effectiveness of increased $p_{\text{stick}}$.

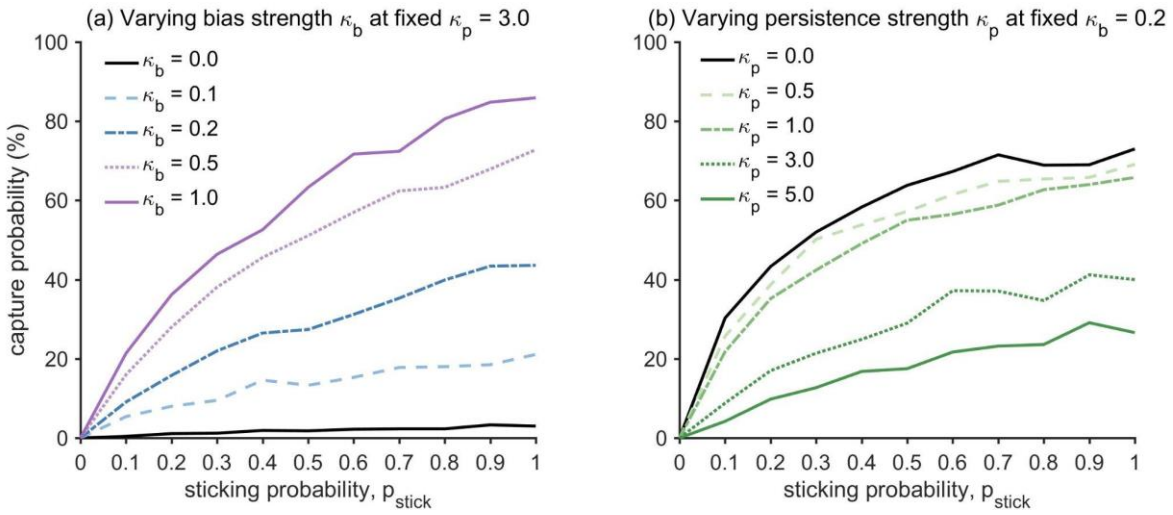



**Figure 6.** Capture probability as a function of the sticking probability $p_{\mathrm{stick}}$ for (a) directional bias strengths $\kappa_b = 0, 0.1, 0.2, 0.5$ and 1, with directional persistence fixed at $\kappa_p = 3$, and for (b) directional persistence strengths $\kappa_p = 0, 0.5, 1, 3$ and 5, with directional bias fixed at $\kappa_b = 0.2$. The panel was square with side length $L = 10$ cm, and capture probabilities were estimated from 1000 independent trajectories for each parameter combination. Release conditions, trajectory duration, and all other movement and post-contact parameters were as in Figure 3.

### 3.5 *Encounter times and search efficiency*

Mean time to first encounter increased with the initial distance from the panel $d$ across most movement regimes (Figure 7). At fixed $\kappa_p = 3$, increasing directional bias substantially reduced encounter time across the full distance range (Figure 7a). Strongly biased trajectories $\kappa_b = 0.5$ and 1 showed relatively smooth, approximately linear increases in encounter time with $d$, whereas weaker bias produced longer and more variable encounter times. In the unbiased case $\kappa_b = 0$, encounter-time estimates became highly irregular and were undefined at several larger distances because few or no trajectories reached the finite panel. Thus, mean encounter times in these cases were based only on the small subset of trajectories that successfully encountered the panel.

At fixed $\kappa_b = 0.2$, mean encounter time also increased with $d$, but declined progressively as directional persistence increased (Figure 7b). Low-persistence trajectories required the longest times to reach the panel, whereas strongly persistent trajectories reached it more rapidly across most distances. The separation among persistence levels was maintained over the distance range, with $\kappa_p = 5$ generally producing the shortest encounter times and $\kappa_p = 0$ the longest. These results show that, among trajectories that successfully encountered the panel, both stronger directional bias and greater persistence reduced the time required for first interception.

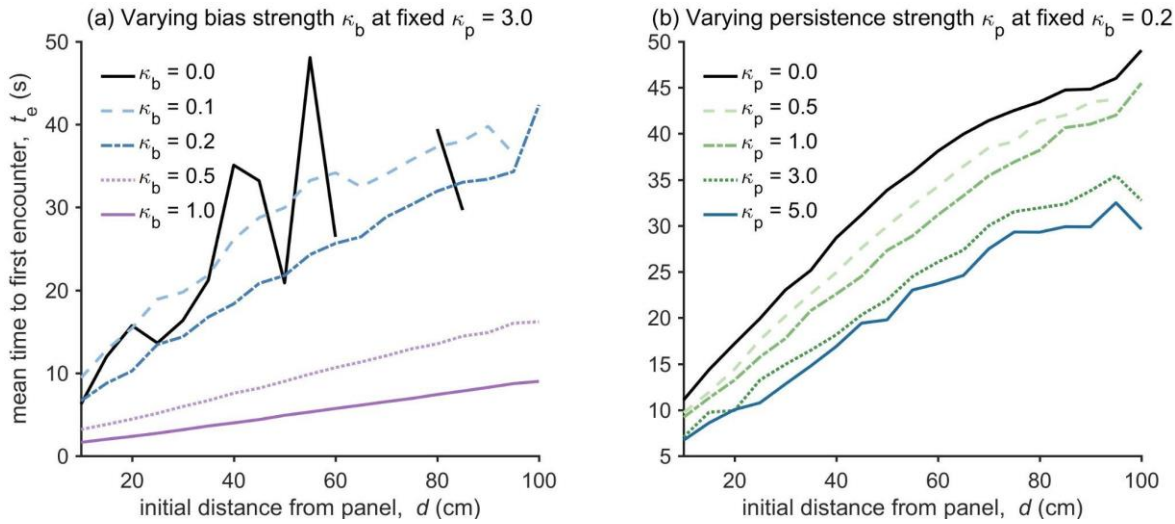



**Figure 7.** Mean time to first panel encounter $t_e$ as a function of the initial distance $d$ from the panel for (a) directional bias strengths $\kappa_b = 0, 0.1, 0.2, 0.5$ and 1, with directional persistence fixed at $\kappa_p = 3$, and for (b) directional persistence strengths $\kappa_p = 0, 0.5, 1, 3$ and 5, with directional bias fixed at $\kappa_b = 0.2$. The panel was square with side length $L = 10$ cm. Encounter time was calculated only for trajectories that intersected the finite panel before edge leakage or escape, and mean encounter times were estimated from 1000 independent trajectories for each parameter combination. Release conditions and all other movement and simulation parameters were as in Figure 3.

### 3.6 *Movement and panel-size effects on edge leakage*

Edge leakage varied jointly with directional persistence, directional bias and panel size (Figure 8). For all panel sizes, leakage showed a non-monotonic dependence on $\kappa_p$ and $\kappa_b$. Leakage was generally low at very weak bias, increased across intermediate bias strengths and declined again at stronger bias. The low leakage under weak directional bias is consistent with relatively few trajectories reaching the panel plane, rather than more effective interception by the trapping surface. Increasing persistence shifted regions of elevated leakage towards higher bias strengths, such that stronger directional bias was required to maintain low leakage as persistence increased. For the smallest panel ($L = 10$ cm), leakage exceeded 50% across a broad region of parameter space and exceeded 75% under some combinations of intermediate bias and moderate-to-high persistence.

Increasing panel size substantially reduced leakage and contracted the regions of high leakage. At $L = 20$ cm, leakage above 50% was largely restricted to intermediate bias combined with moderate-to-high persistence, and the 75% leakage region was absent. At $L = 30$ cm, leakage remained below 50% across almost the entire parameter space, with values above this threshold confined to a small region of intermediate bias and high persistence. Edge leakage therefore depended jointly on movement behaviour and the spatial extent of the trapping surface.

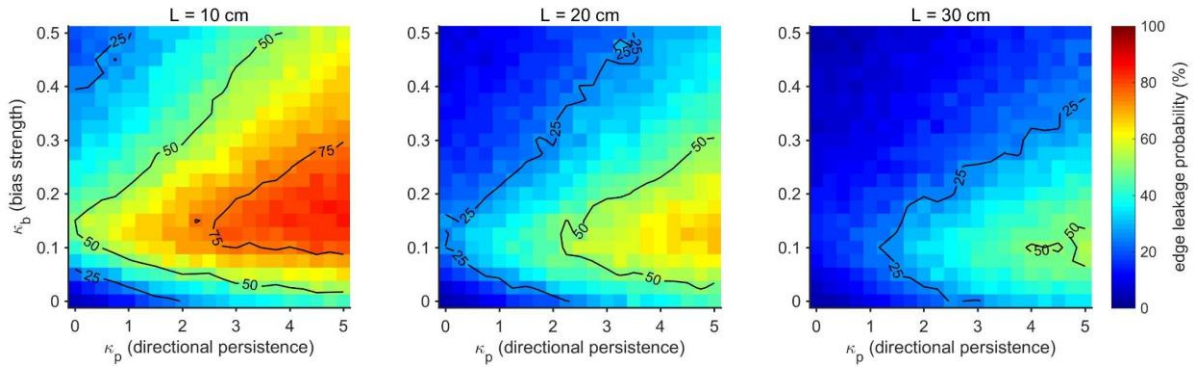



**Figure 8.** Heat maps showing edge leakage probability as a function of directional persistence $\kappa_p$ and directional bias $\kappa_b$ for three square panel sizes: (a) $L = 10$ cm, (b) $L = 20$ cm and (c) $L = 30$ cm. Contours indicate $25\%$, $50\%$ and $75\%$ edge leakage probability, calculated as the proportion of all simulated trajectories that crossed the panel plane outside the trapping surface before any panel contact. Individuals were released at an initial distance $d = 30$ cm from the panel, and edge leakage probabilities were estimated from $1000$ independent trajectories for each parameter combination. Release conditions, trajectory duration and all other movement parameters were as in Figure 3.

## 4. Discussion

The present study builds on animal movement models by applying three-dimensional correlated and biased correlated random walks to flying insects interacting with finite planar surfaces. This approach, for the first time, links movement structure to panel encounter, edge leakage, repeated contact and capture. Our results show that movement persistence and directional bias jointly govern panel encounter and capture, while geometric interception distinguishes successful contact from edge leakage. Larger panels (relative to persistence length) generally increased encounter and capture probabilities but could not compensate for weak attraction. While increased retention enhanced capture, it could not offset low encounter rates and reduced repeated contacts. This approach mechanistically demonstrates the flight processes that could mediate the efficacy of planar traps, in a framework relevant to movement ecology, trapping theory and other contact-driven ecological processes.

Correlated random walks have played a central role in the development of movement ecology by providing a tractable link between individual stepwise behaviour and emergent spatial displacement (Kareiva and Shigesada, 1983; Fagan and Calabrese, 2014). Their appeal lies not in reproducing the full complexity of animal movement, but in providing a mechanistic baseline against which directional persistence, bias and other structured behaviours can be identified. For many years, however, the mathematical properties underpinning this approach—particularly the relationship between path structure and mean squared displacement—were established primarily for movement in two dimensions. Extending these ideas into three-dimensional space required an appropriate treatment of directional changes on the sphere and led to corresponding expressions for the mean squared displacement and sinuosity of balanced three-dimensional correlated random walks (Benhamou, 2018). This theoretical development subsequently supported broad ecological formulations of simple, correlated and biased random walks in three dimensions, together with initial applications to animal trapping and encounter processes (Ahmed et al., 2021), while also reinforcing the importance of such models as baselines for analysing the growing

volume of three-dimensional movement data (Ahmed et al., 2023a). More recently, these foundations have been extended into a general inferential framework for estimating three-dimensional movement and habitat-selection processes from empirical tracking data, including attraction towards multiple directional targets (Klappstein et al., 2026).

According to our results, the probability of encountering a planar surface depended strongly on how individuals moved through three-dimensional space. Directional bias was the main determinant of encounter probability, consistently enhancing capture and indicating that planar traps tend to be more effective when associated with biologically meaningful cues that attract insects (e.g., color and odor; Frye and Dickinson, 2004; Takikawa et al., 2021). Increasing panel size increased encounter probability and substantially reduced edge leakage, but produced limited gains when directional bias was weak, showing that larger surfaces cannot compensate for the absence of attraction toward the target. This suggests that inadvertent capture of non-target insects may also be low even by large traps, provided species-specific attractants are used, as they are unlikely to express directional orientation towards these, though empirical evidence is mixed and indicates variability by taxonomic order of the by-catch (Gonzalez et al., 2020). Larger panels may nevertheless be particularly important for insects exhibiting persistent flight, since a greater trapping area intuitively reduces the probability of trajectories passing beyond the panel boundaries in addition to factors such as trap shape and material (Sbaraglia et al., 2025). Conversely, evidence from riverine tsetse (*Glossina* species within the *palpalis* group) indicates that target effectiveness does not scale proportionally with target area (Esterhuizen et al., 2011); although reductions in target size reduced overall catch size, killing effectiveness per $m^2$ of cloth was greatly improved, highlighting the importance of tailoring trap design to target species flight behaviour and ecology and improve economic efficiencies around trap deployment.

The simulations also showed that greater directional persistence reduced the time to first encounter among trajectories that successfully reached the panel, indicating that straighter movement can facilitate rapid interception when individuals are sufficiently aligned with the target. However, under conditions of weak directional bias, persistent and straighter trajectories were more likely to overshoot the target. Taken together, our results inform how shifts in movement strategy can affect not only how quickly insects encounter a trapping surface, but also whether they encounter it at all, with consequences for trap effectiveness. Understanding the relationships between flight characteristics (including the mechanisms underpinning them) and encounter rates is critical for pest management and biodiversity monitoring, since insects can alter directionality and persistence of their flight depending on behavioral context, which is a product of endogenous state and exogenous stimulation (Reynolds and Frye, 2007; Osborne et al., 2013). For instance, mosquitoes (*Anopheles coluzzii*) in a physiological state primed for blood-feeding will fly with consistent and relatively low angular velocities and weak bias towards planar visual targets in clean air, resulting in low target approach rates, but switch to directionally oriented and more tortuous flight trajectories when host odour is introduced, which produces frequent target approaches (Hawkes and Gibson, 2016). Consequently, trap captures do not necessarily reflect species abundance or species richness in an area alone, as they are also influenced by context-dependent flight activity, which alters the likelihood of individuals encountering the trap according to their directional bias and persistence (Winterbourn and Crowe, 2001; Petrovskii

et al., 2012), and the intrinsic biases of trap designs that influence these. Assuming that trap counts resemble empirical ecological communities without accounting for these behaviours may thus lead to spurious interpretations.

Encounter, however, represents only the first stage of the trapping process, because contact with a panel does not necessarily result in capture. Our simulations showed that imperfect retention reduced capture probability across movement regimes and fundamentally altered the structure of panel interactions. Without retention, strongly biased trajectories frequently contacted the panel multiple times before escaping, whereas retention truncated these trajectories by removing individuals after successful capture. Importantly, increasing retention could not compensate for movement regimes that generated few encounters, demonstrating that capture depends on both the probability of reaching the surface and capture once contact occurs. This distinction has direct relevance to planar trapping methods used for insect monitoring. For example, western flower thrips (*Frankliniella occidentalis*) can escape after initial contact with yellow sticky traps, with escape varying according to adhesive properties (Rehling et al., 2025). In other empirical studies, a similar distinction between attraction, encounter and retention was found in laboratory experiments on the effective capture area of mosquito (*Anopheles coluzzii)* suction traps (Cribellier et al., 2018; Cribellier, 2021) and has been well-characterised in tsetse traps through field research using electric nets to passively and objectively quantify trap interactions (summarised in Torr and Vale, 2015). However, data on such post-contact losses are scarce but important as they can affect the number of individuals retained by a trap and, consequently, the interpretation of trap-based observations, as well as the efficacy of interventions based on pest contact with, but not retention on, surfaces impregnated with insecticides or insect growth regulators, for instance. More generally, separating encounter from capture allows our framework to distinguish low trapping success caused by limited exposure to the trapping surface from low success caused by failure to capture individuals after contact. Inter-species and inter-individual variation in flight behaviour can thus be parameterized according to differences in expression of these two modalities, alongside differences in the retention capabilities of traps themselves.

Although our approach explicitly assesses the implications of key flight behavioural traits for trap efficiency, it is important to acknowledge the myriad biotic and abiotic contexts that the model does not currently integrate and that provide future research avenues. Firstly, while we aimed to demonstrate a generalised framework that applies to various short-range model flight taxa that are commonly targeted by traps, including aphids, whiteflies, thrips, and mosquitoes, variations in flight behaviour can result from both interspecific and intraspecific differences, including those related to different sexes, reproductive statuses, and ontogenic stages (Vance et al., 2009; Rund et al., 2012; Dong et al., 2025). Nevertheless, dipteran flight diversity among species has been shown to be governed by similar aerodynamic principles and scaling laws, allowing for potential application and parameter tailoring to various study systems (Le Roy et al., 2026). Future extensions could account for systematic differences between horizontal and vertical movement, including asymmetries between ascending and descending flight arising from gravitational and aerodynamic constraints (Shen et al., 2018; Walker and Taylor, 2021), as well as distinct flight behaviours such as alternating periods of relatively straight flight and rapid saccadic turns (van Breugel

and Dickinson, 2014; Cribellier et al., 2026), which may influence three-dimensional movement trajectories and subsequent encounters with trapping surfaces. Secondly, as ectotherms, insect behaviours and morphological traits are mediated by environmental conditions, both experienced acutely and over their life history, including abiotic limits for activity. For example, flight performance of the vector mosquito *Aedes aegypti* has been found to be mediated by temperature and humidity regimes (Rowley and Graham, 1968), and fruit fly pests (Tephritidae) exhibit temperature-dependent performance (Malod et al., 2025). Larger-scale weather patterns (i.e., wind) may also mediate insect migration dynamics and subsequent short-range flights in new destinations (Jones et al., 2026). However, detailed assessments of responses within and between species is limited in the vast majority of insect taxa, with thermal performance potentially differing markedly between populations, and typically non-linearly (Fay et al., 2024). Finally, landscape structure and complexity is also likely to shape the evolutionary context in which insect flight behaviours emerge. For example, there are fundamental differences in the host-oriented behaviour of riverine versus savannah species of tsetse flies (Torr et al., 2011), and it is hypothesised that forest groups of the *Simulium damnosum* sensu lato complex of blackflies primarily use odour during host location, in contrast to savannah groups, which are thought to be more reliant on visual stimuli that are more easily observed in open savannah-type landscapes (Thompson, 1977). Trap design may therefore require adaptations to the differential opportunities for insect movement, cue dispersal and cue detection according to landscape structure.

Aside from organismal and environmental context-dependencies, variations related to the trap surface itself (beyond size and shape) could mediate responses. Considering sticky traps, where applications of our models are intuitive given their relevance for monitoring and mass-trapping pests, colouration and texture may substantially mediate attraction and thus flight dynamics towards a focal surface, with the best performing colours likely differing among target species given innate variations in light receptors and sensory structures (Santer, 2014; Santer et al., 2019; Roberts et al., 2025). This means that colour-driven variation among pests likely underpins trap efficacy, and thus could introduce further variability into our model framework (Yudin et al., 1987). The same principles apply considering variations in attractiveness to surfaces, including through the use of bait, or conversely, potential reductions in stickiness or attractiveness over time within traps that dissolve their efficacy. This suite of context-dependencies, while being necessary caveats on our theoretical advance, provides for a fruitful array of research directions to further refine and apply our framework. For example, they may help to reduce non-target effects if resolved traps can be better tailored towards target pest taxa flight traits and their innate surface preferences. Our study also highlights the importance of developing effective ways to distinguish between trap attraction and trap retention, as these processes ultimately determine the efficiency of a given trap design.

In light of these variables, we encourage future applications that refine and validate our model predictions, including assessing the relative efficacy of single versus multiple traps and those of different sizes; as well as experimental trials both in controlled laboratory and in-field scenarios. Calibrating the model against empirical three-dimensional flight trajectories could further improve its biological realism and predictive capabilities. Moreover, applications to other study systems that comprise a three-dimensional movement space,

particularly in aquatic realms, could offer intuitive future avenues to improve monitoring and catches in freshwater and marine settings, considering other taxonomic groups.

## 5. Conclusion

This study contributes to movement ecology and insect trapping research by providing a mechanistic framework linking three-dimensional insect flight behaviour to encounter and capture probabilities on planar surfaces using biased and correlated random walks. Our results demonstrate that panel geometry, directional persistence, directional bias and retention probabilities jointly influence trapping success, with edge leakage representing an additional source of interception failure. Importantly, stronger attraction increased encounters and capture, whereas greater directional persistence generally reduced capture, and improved retention could not compensate for low encounter rates. This approach provides opportunities to improve trap design, refine the interpretation of trap-based monitoring data and inform more targeted monitoring and management strategies for both pest and beneficial insects.

## CRediT authorship contribution statement

**Danish A. Ahmed:** Conceptualization, Formal analysis, Funding acquisition, Investigation, Methodology, Project administration, Software, Supervision, Validation, Visualization, Writing – original draft, Writing – review and editing. **Ross N. Cuthbert:** Writing – original draft, Writing – review and editing. **Isadora E. Fluck:** Writing – original draft, Writing – review and editing. **Frances M. Hawkes:** Writing – original draft, Writing – review and editing. **Gala Garrod:** Writing – review and editing.

## Declaration of competing interest

The authors declare that they have no competing financial interests or personal relationships that could have influenced the work reported in this paper.


## Funding sources

Danish A. Ahmed was supported by Gulf University for Science and Technology, Kuwait. The funder had no role in the study design, analysis, interpretation of results, manuscript preparation, or decision to submit for publication.


## Declaration of generative AI and AI-assisted technologies in the manuscript preparation process

During the preparation of this manuscript, the authors used ChatGPT (OpenAI) to assist with the development and refinement of MATLAB simulation code and to improve the language and readability of the manuscript. The authors subsequently reviewed and verified the code, reviewed and edited the manuscript, and are fully responsible for the accuracy and integrity of the study and its findings.

## Data availability

The MATLAB codes used to perform the simulations and generate the figures presented in this study are publicly available on GitHub (https://github.com/daa119/Movement-surface-interactions-of-flying-insects). An archived version of the code is available on Zenodo (https://doi.org/10.5281/zenodo.23973082).

**Acknowledgements**

We thank Antoine Cribellier (Experimental Zoology Group, Wageningen University & Research, The Netherlands) for helpful comments and constructive feedback on an earlier version of the manuscript.

**References**

Ahmed, D.A., Bailey, J.D., Bonsall, M.B., 2023a. On random walk models as a baseline for animal movement in three-dimensional space. Ecological Modelling 475, 110169. https://doi.org/10.1016/j.ecolmodel.2022.110169

Ahmed, D.A., Beidas, A., Petrovskii, S.V., Bailey, J.D., Bonsall, M.B., Hood, A.S.C., Byers, J.A., Hudgins, E.J., Russell, J.C., Růžičková, J., Bodey, T.W., Renault, D., Bonnaud, E., Haubrock, P.J., Soto, I., Haase, P., 2023b. Simulating capture efficiency of pitfall traps based on sampling strategy and the movement of ground-dwelling arthropods. Methods in Ecology and Evolution 14, 2827–2843. https://doi.org/10.1111/2041-210X.14174

Ahmed, D.A., Benhamou, S., Bonsall, M.B., Petrovskii, S.V., 2021. Three-dimensional random walk models of individual animal movement and their application to trap counts modelling. Journal of Theoretical Biology 524, 110728. https://doi.org/10.1016/j.jtbi.2021.110728

Ahmed, D.A., Petrovskii, S.V., 2019. Analysing the impact of trap shape and movement behaviour of ground-dwelling arthropods on trap efficiency. Methods in Ecology and Evolution 10, 1246–1264. https://doi.org/10.1111/2041-210X.13207

Batista, E.P.A., Mapua, S.A., Ngowo, H., Matowo, N.S., Melo, E.F., Paixão, K.S., Eiras, A.E., Okumu, F.O., 2019. Videographic analysis of flight behaviours of host-seeking Anopheles arabiensis towards BG-Malaria trap. PLoS ONE 14, e0220563. https://doi.org/10.1371/journal.pone.0220563

Benhamou, S., 2018. Mean squared displacement and sinuosity of three-dimensional random search movements. arXiv. https://doi.org/10.48550/arXiv.1801.02435

Benthall, K.J., Avila, N., Leake, L.B., Althoff, E.R., Nielsen, A.L., Rice, K.B., 2022. Comparison of parasitoid retention on yellow sticky card traps. Florida Entomologist 105, 167–169. https://doi.org/10.1653/024.105.0210

Bessell, P.R., Esterhuizen, J., Lehane, M.J., Longbottom, J., Mugenyi, A., Selby, R., Tirados, I., Torr, S.J., Waiswa, C., Wamboga, C., Hope, A., 2021. Estimating the impact of Tiny Targets in reducing the incidence of Gambian sleeping sickness in the North-west Uganda focus. Parasites & Vectors 14, 410. https://doi.org/10.1186/s13071-021-04889-x

Bredt, B.H., Tripet, F., Müller, P., 2025. Revealing complex mosquito behaviour: a review of current automated video tracking systems suitable for tracking mosquitoes in the field. Parasites & Vectors 18, 66. https://doi.org/10.1186/s13071-025-06666-6

Butail, S., Manoukis, N., Diallo, M., Ribeiro, J.M., Lehmann, T., Paley, D.A., 2012. Reconstructing the flight kinematics of swarming and mating in wild mosquitoes. Journal of the Royal Society Interface 9, 2624–2638. https://doi.org/10.1098/rsif.2012.0150

Byers, J.A., 2009. Modeling distributions of flying insects: effective attraction radius of pheromone in two and three dimensions. Journal of Theoretical Biology 256, 81–89. https://doi.org/10.1016/j.jtbi.2008.09.002

Byers, J.A., 2012. Estimating insect flight densities from attractive trap catches and flight height distributions. Journal of Chemical Ecology 38, 592–601. https://doi.org/10.1007/s10886-012-0116-8

Carnaghi, M., Belmain, S.R., Hopkins, R.J., Hawkes, F.M., 2021. Multimodal synergisms in host stimuli drive landing response in malaria mosquitoes. Scientific Reports 11, 7379. https://doi.org/10.1038/s41598-021-86772-4

Carnaghi, M., Mandelli, F., Feugère, L., Joiner, J., Young, S., Belmain, S.R., Hopkins, R.J., Hawkes, F.M., 2024. Visual and thermal stimuli modulate mosquito-host contact with implications for improving malaria vector control tools. iScience 27, 108578. https://doi.org/10.1016/j.isci.2023.108578

Chen, C.-H., Chiang, A.-S., Tsai, H.-Y., 2021. Three-dimensional tracking of multiple small insects by a single camera. Journal of Insect Science 21, 14. https://doi.org/10.1093/jisesa/ieab079

Chen, H., Li, M., Månefjord, H., Travers, P., Salvador, J., Müller, L., Dreyer, D., Alison, J., Høye, T.T., Hu, G., Warrant, E., Brydegaard, M., 2024. Lidar as a potential tool for monitoring migratory insects. iScience 27, 109588. https://doi.org/10.1016/j.isci.2024.109588

Cribellier, A., 2021. Biomechanics of flying mosquitoes during capture and escape. PhD thesis, Wageningen University. https://doi.org/10.18174/552797

Cribellier, A., Poda, B.S., Dabiré, R.K., Diabaté, A., Roux, O., Muijres, F.T., 2026. The complex swarming dynamics of malaria mosquitoes emerge from simple minimally-interactive behavioral rules. PLoS Computational Biology 22, e1014685. https://doi.org/10.1371/journal.pcbi.1014685

Cribellier, A., Spitzen, J., Fairbairn, H., van de Geer, C., van Leeuwen, J.L., Muijres, F.T., 2020. Lure, retain, and catch malaria mosquitoes. How heat and humidity improve odour-baited trap performance. Malaria Journal 19, 357. https://doi.org/10.1186/s12936-020-03403-5

Cribellier, A., van Erp, J.A., Hiscox, A., Lankheet, M.J., van Leeuwen, J.L., Spitzen, J., Muijres, F.T., 2018. Flight behaviour of malaria mosquitoes around odour-baited traps: capture and escape dynamics. Royal Society Open Science 5, 180246. https://doi.org/10.1098/rsos.180246

da Cruz Ferreira, D.A., Degener, C.M., de Almeida Marques-Toledo, C., Bendati, M.M., Fetzer, L.O., Teixeira, C.P., Eiras, Á.E., 2017. Meteorological variables and mosquito monitoring are good predictors for infestation trends of Aedes aegypti, the vector of dengue, chikungunya and Zika. Parasites & Vectors 10, 78. https://doi.org/10.1186/s13071-017-2025-8

Dedic, E., Henry, D., Lihoreau, M., Aubert, H., 2024. 3D detection of flying insects from a millimeter-wave radar imaging system. Computers and Electronics in Agriculture 226, 109357. https://doi.org/10.1016/j.compag.2024.109357

Dong, L., Bradford, E.F., Barnett, J.M., Duvall, L.B., 2025. Post-biting behavioral reprogramming underlies reproductive efficiency in Aedes aegypti mosquitoes. Cell Reports 44, 116663. https://doi.org/10.1016/j.celrep.2025.116663

El-Sayed, A.M., Suckling, D.M., Wearing, C.H., Byers, J.A., 2006. Potential of mass trapping for long-term pest management and eradication of invasive species. Journal of Economic Entomology 99, 1550–1564. https://doi.org/10.1093/jee/99.5.1550

Epsky, N.D., Morrill, W.L., Mankin, R.W., 2008. Traps for capturing insects, in: Encyclopedia of Entomology. Springer, Dordrecht, pp. 3887–3901. https://doi.org/10.1007/978-1-4020-6359-6_2523

Esterhuizen, J., Rayaisse, J.B., Tirados, I., Mpiana, S., Solano, P., Vale, G.A., Lehane, M.J., Torr, S.J., 2011. Improving the cost-effectiveness of visual devices for the control of riverine tsetse flies, the major vectors of human African trypanosomiasis. PLoS Neglected Tropical Diseases 5, e1257. https://doi.org/10.1371/journal.pntd.0001257

Fagan, W.F., Calabrese, J.M., 2014. The correlated random walk and the rise of movement ecology. Bulletin of the Ecological Society of America 95, 204–206. https://doi.org/10.1890/0012-9623-95.3.204

887 Fay, R.L., Cruz-Loya, M., Keyel, A.C., Price, D.C., Zink, S.D., Mordecai, E.A., Ciota, A.T., 2024.
888 Population-specific thermal responses contribute to regional variability in arbovirus
889 transmission with changing climates. iScience 27, 109934.
890 https://doi.org/10.1016/j.isci.2024.109934
891 Frye, M.A., Dickinson, M.H., 2004. Closing the loop between neurobiology and flight behavior in
892 Drosophila. Current Opinion in Neurobiology 14, 729–736.
893 https://doi.org/10.1016/j.conb.2004.10.004
894 Gonzalez, V.H., Osborn, A.L., Brown, E.R., Pavlick, C.R., Enríquez, E., Tscheulin, T., Petanidou, T.,
895 Hranitz, J.M., Barthell, J.F., 2020. Effect of pan trap size on the diversity of sampled bees and
896 abundance of bycatch. Journal of Insect Conservation 24, 409–420.
897 https://doi.org/10.1007/s10841-020-00224-4
898 Hawkes, F., Gibson, G., 2016. Seeing is believing: the nocturnal malarial mosquito Anopheles
899 coluzzii responds to visual host-cues when odour indicates a host is nearby. Parasites &
900 Vectors 9, 320. https://doi.org/10.1186/s13071-016-1609-z
901 Heinz, K.M., Parrella, M.P., Newman, J.P., 1992. Time-efficient use of yellow sticky traps in
902 monitoring insect populations. Journal of Economic Entomology 85, 2263–2269.
903 https://doi.org/10.1093/jee/85.6.2263
904 Hohbein, R.R., Conway, C.J., 2018. Pitfall traps: a review of methods for estimating arthropod
905 abundance. Wildlife Society Bulletin 42, 597–606. https://doi.org/10.1002/wsb.928
906 Hurst, A.L., O'Brien, A.L., Miller, N.D., Peachey, A.M.W., Yoder, J.M., de Faveri, S.G., Cheesman,
907 J., Manoukis, N.C., Siderhurst, M.S., 2024. Tracking and modeling the movement of
908 Queensland fruit flies, Bactrocera tryoni, using harmonic radar in papaya fields. Scientific
909 Reports 14, 17521. https://doi.org/10.1038/s41598-024-67372-4
910 Ings, T.C., Chittka, L., 2008. Speed-accuracy tradeoffs and false alarms in bee responses to cryptic
911 predators. Current Biology 18, 1520–1524. https://doi.org/10.1016/j.cub.2008.07.074
912 Isaacs, R., Willis, M.A., Byrne, D.N., 1999. Modulation of whitefly take-off and flight orientation by
913 wind speed and visual cues. Physiological Entomology 24, 311–318.
914 https://doi.org/10.1046/j.1365-3032.1999.00144.x
915 Jimenez-Vallejo, D., Gonzalez-Olvera, G., Che-Mendoza, A., Medina-Barreiro, A., del Castillo-
916 Centeno, F., Crews, S.A., Bastille-Rousseau, G., Manrique-Saide, P., Vazquez-Prokopec, G.,
917 2026. Drivers of mosquito free-flight and resting behavior indoors. Preprint.
918 https://doi.org/10.64898/2026.02.11.705377
919 Jones, C.M., Reynolds, D.R., Wipf, N.C., Chapman, J.W., Lehmann, T., 2026. The migratory
920 behaviour of salt marsh mosquitoes: revisiting the evidence. Medical and Veterinary
921 Entomology 40, 215–220. https://doi.org/10.1111/mve.70021
922 Kareiva, P.M., Shigesada, N., 1983. Analyzing insect movement as a correlated random walk.
923 Oecologia 56, 234–238. https://doi.org/10.1007/BF00379695
924 Kirkeby, C., Wellenreuther, M., Brydegaard, M., 2016. Observations of movement dynamics of flying
925 insects using high resolution lidar. Scientific Reports 6, 29083.
926 https://doi.org/10.1038/srep29083
927 Klappstein, N., Michelot, T., Togunov, R., Mills Flemming, J., 2026. Three-dimensional correlated
928 random walks for animal movement and habitat selection. Ecology Letters 29, e70414.
929 https://doi.org/10.1111/ele.70414
930 Le Roy, C., Bharathi, I., Engels, T., Muijres, F.T., 2026. Dipteran flight diversity is shaped by
931 aerodynamic constraints, scaling, and evolutionary trade-offs. PLoS Biology 24, e3003473.
932 https://doi.org/10.1371/journal.pbio.3003473

Lennox, R.J., Adam, T., Riha, M., Klappstein, N., Monk, C.T., Vollset, K.W., Beumer, L.T., 2025. Movement in 3D: novel opportunities for understanding animal behaviour and space use. Ethology 131, e13529. https://doi.org/10.1111/eth.13529

Lima-Camara, T.N., Bruno, R.V., Luz, P.M., Castro, M.G., Lourenço-de-Oliveira, R., Sorgine, M.H.F., Peixoto, A.A., 2011. Dengue infection increases the locomotor activity of Aedes aegypti females. PLoS ONE 6, e17690. https://doi.org/10.1371/journal.pone.0017690

Lindh, J.M., Torr, S.J., Vale, G.A., Lehane, M.J., 2009. Improving the cost-effectiveness of artificial visual baits for controlling the tsetse fly Glossina fuscipes fuscipes. PLoS Neglected Tropical Diseases 3, e474. https://doi.org/10.1371/journal.pntd.0000474

MacLeod, C.D., Luong, L.T., 2024. Navigating the landscape of fear: fruit flies exhibit distinct antipredator and antiparasite defensive behaviors. Ecology 105, e4397. https://doi.org/10.1002/ecy.4397

Malod, K., Bali, E.D., Gledel, C., Dieudonne, E., Moquet, L., Bierman, A., Bataka, E., Rodovitis, V., Weldon, C.W., Karsten, M., Delatte, H., Papadopoulos, N.T., Terblanche, J.S., 2025. Effects of past and current temperatures on the flight performance of invasive pest fruit flies (Diptera: Tephritidae): climate change may facilitate movements of tropical species to higher latitudes. Functional Ecology 39, 3139–3151. https://doi.org/10.1111/1365-2435.70165

Manzi, S., Nelli, L., Fortuna, C., Severini, F., Toma, L., Di Luca, M., Michelutti, A., Bertola, M., Gradoni, F., Toniolo, F., Sgubin, S., Lista, F., Pazienza, M., Montarsi, F., Pombi, M., 2023. A modified BG-Sentinel trap equipped with FTA card as a novel tool for mosquito-borne disease surveillance: a field test for flavivirus detection. Scientific Reports 13, 12840. https://doi.org/10.1038/s41598-023-39857-1

Mardia, K.V., Jupp, P.E., 2000. Directional statistics. John Wiley & Sons, Chichester.

Martínez-Pérez, S., Galante, E., Micó, E., 2022. Sex specificity of dispersal behaviour and flight morphology varies among tree hollow beetle species. Movement Ecology 10, 41. https://doi.org/10.1186/s40462-022-00340-7

Miller, J.R., Adams, C.G., Schenker, J.H., Weston, P.A., 2015. Trapping of small organisms moving randomly: principles and applications to pest monitoring and management. SpringerBriefs in Ecology. Springer International Publishing, Cham. https://doi.org/10.1007/978-3-319-12994-5

Oram, T.B., Card, G.M., 2022. Context-dependent control of behavior in Drosophila. Current Opinion in Neurobiology 73, 102523. https://doi.org/10.1016/j.conb.2022.02.003

Osborne, J.L., Smith, A., Clark, S.J., Reynolds, D.R., Barron, M.C., Lim, K.S., Reynolds, A.M., 2013. The ontogeny of bumblebee flight trajectories: from naïve explorers to experienced foragers. PLoS ONE 8, e78681. https://doi.org/10.1371/journal.pone.0078681

Petrovskii, S., Bearup, D., Ahmed, D.A., Blackshaw, R., 2012. Estimating insect population density from trap counts. Ecological Complexity 10, 69–82. https://doi.org/10.1016/j.ecocom.2011.10.002

Petrovskii, S., Petrovskaya, N., Bearup, D., 2014. Multiscale approach to pest insect monitoring: random walks, pattern formation, synchronization, and networks. Physics of Life Reviews 11, 467–525. https://doi.org/10.1016/j.plrev.2014.02.001

Pobozniak, M., Tokarz, K., Musynov, K., 2020. Evaluation of sticky trap colour for thrips (Thysanoptera) monitoring in pea crops (Pisum sativum L.). Journal of Plant Diseases and Protection 127, 307–321. https://doi.org/10.1007/s41348-020-00301-5

Polidori, C., Piwczynski, M., Ronchetti, F., Johnston, N.P., Szpila, K., 2022. Host-trailing satellite flight behaviour is associated with greater investment in peripheral visual sensory system in miltogrammine flies. Scientific Reports 12, 2773. https://doi.org/10.1038/s41598-022-06704-8

Radcliffe, E.B., Hutchison, W.D., Cancelado, R.E., 2008. Integrated pest management: concepts, tactics, strategies and case studies. Cambridge University Press, Cambridge.
Rehling, L., Raaz, W., Vaske, J., Döring, T., 2025. Do we need a scientific standard design for yellow sticky traps? Journal of Applied Entomology 149, 1084–1089. https://doi.org/10.1111/jen.13439
Reynolds, A.M., Frye, M.A., 2007. Free-flight odor tracking in Drosophila is consistent with an optimal intermittent scale-free search. PLoS ONE 2, e354. https://doi.org/10.1371/journal.pone.0000354
Reynolds, A.M., Rhodes, C.J., 2009. The Lévy flight paradigm: random search patterns and mechanisms. Ecology 90, 877–887. https://doi.org/10.1890/08-0153.1
Roberts, N.S., Ndayiragije, J.C., Özek, T., Butt, T.M., Karaca, İ., Shah, F., Allen, W.L., 2025. Visual modelling can optimise sticky trap design for simultaneous monitoring of multiple species of insect pests. Scientific Reports 15, 17280. https://doi.org/10.1038/s41598-025-01954-8
Rowley, W.A., Graham, C.L., 1968. The effect of temperature and relative humidity on the flight performance of female Aedes aegypti. Journal of Insect Physiology 14, 1251–1257. https://doi.org/10.1016/0022-1910(68)90018-8
Rund, S.S.C., Lee, S.J., Bush, B.R., Duffield, G.E., 2012. Strain- and sex-specific differences in daily flight activity and the circadian clock of Anopheles gambiae mosquitoes. Journal of Insect Physiology 58, 1609–1619. https://doi.org/10.1016/j.jinsphys.2012.09.016
Santer, R.D., 2014. A colour opponent model that explains tsetse fly attraction to visual baits and can be used to investigate more efficacious bait materials. PLoS Neglected Tropical Diseases 8, e3360. https://doi.org/10.1371/journal.pntd.0003360
Santer, R.D., Vale, G.A., Tsikire, D., Torr, S.J., 2019. Optimising targets for tsetse control: taking a fly's-eye-view to improve the colour of synthetic fabrics. PLoS Neglected Tropical Diseases 13, e0007905. https://doi.org/10.1371/journal.pntd.0007905
Sbaraglia, C., Holm, I.M., Sverdrup-Thygeson, A., Åström, J., Birkemoe, T., 2025. The shape and material of the flight interception trap matter for beetle sampling. Journal of Applied Entomology 149, 1467–1477. https://doi.org/10.1111/jen.13477
Shen, C., Liu, Y., Sun, M., 2018. Lift and power in fruitflies in vertically-ascending flight. Bioinspiration & Biomimetics 13, 056008. https://doi.org/10.1088/1748-3190/aad212
Somerville, A.G.T., Gleave, K., Jones, C.M., Reimer, L.J., 2019. The consequences of Brugia malayi infection on the flight and energy resources of Aedes aegypti mosquitoes. Scientific Reports 9, 18449. https://doi.org/10.1038/s41598-019-54819-2
Southwood, T.R.E., 1978. Ecological methods, 2nd ed. Chapman and Hall, London.
Spitzen, J., Spoor, C.W., Grieco, F., ter Braak, C., Beeuwkes, J., van Brugge, S.P., Kranenbarg, S., Noldus, L.P.J.J., van Leeuwen, J.L., Takken, W., 2013. A 3D analysis of flight behavior of Anopheles gambiae sensu stricto malaria mosquitoes in response to human odor and heat. PLoS ONE 8, e62995. https://doi.org/10.1371/journal.pone.0062995
Stiemer, L.N., Thoma, A., Braun, C., 2023. MBT3D: deep learning based multi-object tracker for bumblebee 3D flight path estimation. PLoS ONE 18, e0291415. https://doi.org/10.1371/journal.pone.0291415
Sun, C., Gaydecki, P., 2021. A visual tracking system for honey bee (Hymenoptera: Apidae) 3D flight trajectory reconstruction and analysis. Journal of Insect Science 21, 17. https://doi.org/10.1093/jisesa/ieab023
Takikawa, Y., Nonomura, T., Sonoda, T., Matsuda, Y., 2021. Developing a phototactic electrostatic insect trap targeting whiteflies, leafminers, and thrips in greenhouses. Insects 12, 960. https://doi.org/10.3390/insects12110960

Tallon, A.K., Lorenzo, M.G., Moreira, L.A., Martinez Villegas, L.E., Hill, S.R., Ignell, R., 2020. Dengue infection modulates locomotion and host seeking in Aedes aegypti. PLoS Neglected Tropical Diseases 14, e0008531. https://doi.org/10.1371/journal.pntd.0008531

Thompson, B.H., 1977. Studies on the attraction of Simulium damnosum s.l. (Diptera: Simuliidae) to its hosts. III. Experiments with animal-baited traps. Tropenmedizin und Parasitologie 28, 226–228.

Torr, S.J., Chamisa, A., Vale, G.A., Lehane, M.J., Lindh, J.M., 2011. Responses of tsetse flies, Glossina morsitans morsitans and Glossina pallidipes, to baits of various size. Medical and Veterinary Entomology 25, 365–369. https://doi.org/10.1111/j.1365-2915.2011.00947.x

Torr, S.J., Vale, G.A., 2015. Know your foe: lessons from the analysis of tsetse fly behaviour. Trends in Parasitology 31, 95–99. https://doi.org/10.1016/j.pt.2014.12.010

van Breugel, F., Dickinson, M.H., 2014. Plume-tracking behavior of flying Drosophila emerges from a set of distinct sensory-motor reflexes. Current Biology 24, 274–286. https://doi.org/10.1016/j.cub.2013.12.023

van Breugel, F., Riffell, J., Fairhall, A., Dickinson, M.H., 2015. Mosquitoes use vision to associate odor plumes with thermal targets. Current Biology 25, 2123–2129. https://doi.org/10.1016/j.cub.2015.06.046

van Klink, R., August, T., Bas, Y., Bodesheim, P., Bonn, A., Fossøy, F., Høye, T.T., Jongejans, E., Menz, M.H.M., Miraldo, A., Roslin, T., Roy, H.E., Ruczyński, I., Schigel, D., Schäffler, L., Sheard, J.K., Svenningsen, C., Tschan, G.F., Wäldchen, J., Zizka, V.M.A., Åström, J., Bowler, D.E., 2022. Emerging technologies revolutionise insect ecology and monitoring. Trends in Ecology & Evolution 37, 872–885. https://doi.org/10.1016/j.tree.2022.06.001

van Klinken, R.D., Gladish, D.W., Manoukis, N.C., Caley, P., Hill, M.P., 2023. Simulation to investigate site-based monitoring of pest insect species for trade. Journal of Economic Entomology 116, 1296–1306. https://doi.org/10.1093/jee/toad112

Vance, J.T., Williams, J.B., Elekonich, M.M., Roberts, S.P., 2009. The effects of age and behavioral development on honey bee (Apis mellifera) flight performance. Journal of Experimental Biology 212, 2604–2611. https://doi.org/10.1242/jeb.028100

Vaxenburg, R., Siwanowicz, I., Merel, J., Robie, A.A., Morrow, C., Novati, G., Stefanidi, Z., Both, G.-J., Card, G.M., Reiser, M.B., Botvinick, M.M., Branson, K.M., Tassa, Y., Turaga, S.C., 2025. Whole-body physics simulation of fruit fly locomotion. Nature 643, 1312–1320. https://doi.org/10.1038/s41586-025-09029-4

Wainwright, C.E., Stepanian, P.M., Reynolds, D.R., Reynolds, A.M., 2017. The movement of small insects in the convective boundary layer: linking patterns to processes. Scientific Reports 7, 5438. https://doi.org/10.1038/s41598-017-04503-0

Walker, S.M., Taylor, G.K., 2021. A semi-empirical model of the aerodynamics of manoeuvring insect flight. Journal of the Royal Society Interface 18, 20210103. https://doi.org/10.1098/rsif.2021.0103

Winterbourn, M.J., Crowe, A.L.M., 2001. Flight activity of insects along a mountain stream: is directional flight adaptive? Freshwater Biology 46, 1479–1489. https://doi.org/10.1046/j.1365-2427.2001.00766.x

Yudin, L.S., Mitchell, W.C., Cho, J.J., 1987. Color preference of thrips (Thysanoptera: Thripidae) with reference to aphids (Homoptera: Aphididae) and leafminers in Hawaiian lettuce farms. Journal of Economic Entomology 80, 51–55. https://doi.org/10.1093/jee/80.1.51

Zuo, C., Fei, C., Cohen, A.E., Kim, S., Cardé, R.T., Dunkel, J., Hu, D.L., 2026. Predicting mosquito flight behavior using Bayesian dynamical systems learning. Science Advances 12, eadz7063. https://doi.org/10.1126/sciadv.adz7063